Theoretical study on electron-free radical collisions: An application to SiH and SiF

M.-T. Lee,[1] M. F. Lima,[1] Antonio M. C. Sobrinho,[2,3] and I. Iga[1]
[1]*Departamento de Química, UFSCar, 13565-905 São Carlos, São Paulo, Brazil*
[2]*Departamento de Física, UFSCar, 13565-905 São Carlos, São Paulo, Brazil*
[3]*Departamento de Física do Estado Sólido, UFBa, Salvador, Bahia, Brazil*
(Received 16 July 2002; published 6 December 2002)

We present a theoretical study of electron collisions on SiH and SiF free radicals in the low- and intermediate-energy range. More specifically, calculated elastic differential, integral and momentum transfer cross sections as well as grand total (elastic and inelastic) and absorption cross sections are reported in the (1–500)-eV energy range. A complex optical potential is used to represent the electron-radical interaction while the Schwinger variational iterative method combined with the distorted-wave approximation is used to solve the scattering equations. Comparisons were made between the calculated cross sections for SiH and SiF as well as with the existing experimental and theoretical data for electron scattering by silane molecule. Some interesting aspects of this comparison are discussed here.

DOI: 10.1103/PhysRevA.66.062703 PACS number(s): 34.80.Bm

I. INTRODUCTION

Electron-molecule collisions play an important role in physical and chemical processes involved in a number of applications such as lasers [1], gas discharges, plasmas [2], and magnetohydrodynamics power generation [3]. In particular, interest in electron collisions with highly reactive radicals such as CH_x, CF_x, $(x=1,2,3)$, etc., has grown recently, in view of their importance in the development of plasma devices. On the other hand, it is surprising that the investigation on radicals such as SiH_x and SiF_x $(x=1,2,3)$ is scarce. It is well known that the plasma etching of silicon is a main process used in the semiconductor and microelectronic industries. There, SiF_x radicals are present in the reacting media. Moreover, SiH_4 is also frequently used in technological processing plasmas for deposition purposes such as amorphous silicon films [4–6] and silicon-carbon diamondlike films [7,8]. Therefore, electron interaction with the SiH_x and SiF_x radicals is certainly important and should affect the properties of the processing plasma. In this sense, the knowledge of various cross sections of electron collision with these radicals are relevant for understanding of the chemistry involved in discharge plasmas. Unfortunately, experimental determination of cross sections for electron interaction with highly reactive radicals is difficult. Only recently, limited electron-impact total ionization cross sections (TICS's) were reported for some of these radicals [9,10]. To our knowledge, no other type of electron-scattering cross-section measurements (elastic and inelastic, differential, and integral, grand total, etc.) were ever reported in the literature. Therefore, theoretical calculation of these cross sections is presently an important manner to fill this lacuna. Recently, e^--radical collisions have been a subject of increasing number of theoretical investigations. Joshipura and Vinodkumar [11] and Joshipura *et al.* [12] have reported grand total cross sections (TCS's) and total absorption cross sections (TACS's) for electron scattering by several CH_x, NH_x, and OH radicals in the intermediate- and high-energy range. A complex optical potential for electron-atom interaction combined with the additivity rule was used in their calculations. Also, Baluja *et al.* [13] and Baluja and Msezane [14] studied low-energy electron collisions with ClO and CH using the *R*-matrix method. More recently, electron scattering by CH and CF in a wide incident energy range were reported by Lee and co-workers [15,16]. Nevertheless, no theoretical investigation was reported for silicon fluoride and silicon hydride radicals.

In this work we present a comparative study on electron scattering by SiH and SiF covering a wide incident energy range. Specifically, calculated elastic differential cross sections (DCS's), integral cross sections (ICS's), and momentum transfer cross sections (MTCS's) as well as TCS's and TACS's for electron impact energies ranging from 1 to 500 eV are presented. The calculated results at low incident energies (below 20 eV) may have some applications in discharge plasma studies. From the fundamental point of view, the knowledge of several electron-scattering cross sections in a wide energy range is also relevant.

The present study made use of a complex optical potential to represent the electron-radical interaction dynamics, while a combination of the Schwinger variational iterative method (SVIM) [17,18] and the distorted-wave approximation (DWA) [19–21] is used to solve the scattering equations. This procedure has already been applied to treat electron scattering by a number of molecules [22–26] and has proven to provide reliable DCS's, ICS's, and MTCS's over a wide energy range. Moreover, although the present study is unable to provide directly electron-impact TICS's, the difference between the calculated TCS's and ICS's would provide an estimate of the TACS's, which account for all inelastic contributions including both excitation and ionization processes. Recently, Joshipura *et al.* [12] have observed that, for a set of molecules, the ionization dominates the inelastic processes. The TICS's correspond to about 70% of the TACS's at energies around 100 eV, and goes to near 100% for energies above 300 eV. Therefore, a comparison of the present calculated TACS's with experimental and calculated TICS's is meaningful and would provide insights of the electron-impact ionization dynamics.

The organization of this paper is as follows. In Sec. II, we describe briefly the theory used and also give some details of

the calculation. In Sec. III, we compare our calculated results with experimental data and other theoretical results reported in the literature. A brief concluding remark is also summarized in Sec. IV.

II. THEORY AND CALCULATIONS

Since the details of the SVIM and the DWA have already been presented in previous works [17–21], only a brief outline will be given here. Within the adiabatic-nuclei-rotation framework, the DCS's for the excitation from an initial rotational level j_0 to a final level j is given by

$$\frac{d\sigma}{d\Omega}(j\leftarrow j_0)=\frac{k_j}{k_0}\frac{1}{(2j_0+1)}\sum_{m_j m_{j_0}}|\langle jm_j|f|j_0m_{j_0}\rangle|^2, \quad (1)$$

where j_0, $m_{j_0}(j,m_j)$ are the rotational quantum numbers of the initial (final) rotational state, f is the laboratory-frame (LF) electronic part of the scattering amplitude, and k_0 and k_j are the linear-momentum magnitudes of the incident and the scattered electrons, respectively. Using the rigid-rotor approximation, the wave function for a given $|jm_j\rangle$ is

$$|jm_j\rangle=\left[\frac{(2j+1)}{8\pi^2}\right]^{1/2}D^j_{m_j0}(\hat{R}), \quad (2)$$

where $D^j_{m_j0}$ are the usual finite rotational matrix elements.

The partial-wave expansion of the rotational-excitation scattering amplitude is given by

$$\begin{aligned}\langle jm_j|f|j_0m_{j_0}\rangle=&4\pi[(2j+1)(2j_0+1)]^{1/2}\sum_{ll'm}(-1)^{m+m_{j_0}+1}i^{l-l'}T_{ll'm}Y_{l'm_j-m_{j_0}}\\&\times\sum_L(2L+1)^{-1}(l0l'm_j-m_{j_0}|ll'Lm_j-m_{j_0})(l-ml'm|ll'L0)(j-m_jj_0m_{j_0}|jj_0Lm_{j_0}-m_j)\\&\times(j0j_00|jj_0L0),\end{aligned} \quad (3)$$

where $T_{ll'm}$ are the scattering T-matrix elements, Y_{lm} the usual spherical harmonics, and $(l_1m_1l_2m_2|l_1l_2l_3m_3)$ are Clebsch-Gordan coefficients.

The rotationally unresolved DCS's for elastic e^--radical scattering are calculated via a summation of all rotationally resolved DCS's

$$\frac{d\sigma}{d\Omega}=\sum_{j=0}\frac{d\sigma}{d\Omega}(j\leftarrow j_0). \quad (4)$$

In the present study, the e^--radical scattering dynamics is represented by a complex optical potential, given by

$$V_{opt}(\vec{r})=V^{SEP}(\vec{r})+iV_{ab}(\vec{r}), \quad (5)$$

where V^{SEP} is the real part of the interaction potential composed by static (V_{st}), exchange (V_{ex}), and correlation-polarization (V_{cp}) contributions, whereas V_{ab} is an absorption potential. V_{st} and V_{ex} are obtained exactly from a Hartree-Fock self-consistent-field (SCF) target wave function. A parameter-free model potential introduced by Padial and Norcross [27] is used to account for the correlation-polarization contributions. In this model, a short-range correlation potential between the scattering and the target electrons is defined in an inner region and a long-range polarization potential in an outer region. The first crossing of the correlation and polarization potential curves defines the inner and the outer regions. The correlation potential is calculated by a free-electron-gas model, derived from the target electronic density according to Eq. (9) of the paper of Padial and Norcross [27]. In addition, the asymptotic form of the polarization potential is used for the long-range electron-target interaction. Since there are no reported experimental dipole polarizabilities for these radicals, the calculated open-shell Restrict-Hartree-Fock (ROHF) values of $\alpha_0=37.483$ a.u. and $\alpha_2=0.546$ a.u. for SiH and $\alpha_0=33.662$ a.u. and $\alpha_2=3.092$ a.u. for SiF, were used to generate the asymptotic form of V_{cp}. No cutoff or other adjusted parameters are needed for the calculation of V_{cp}.

The absorption potential V_{ab} in Eq. (5) is given as

$$\begin{aligned}V_{ab}(\vec{r})=&-\rho(\vec{r})(T_L/2)^{1/2}(8\pi/5k^2k_F^3)\\&\times H(\alpha+\beta-k_F^2)(A+B+C),\end{aligned} \quad (6)$$

where

$$T_L=k^2-V^{SEP}, \quad (7)$$

$$A=5k_F^3/(\alpha-k_F^2), \quad (8)$$

$$B=-k_F^3[5(k^2-\beta)+2k_F^2]/(k^2-\beta)^2, \quad (9)$$

and

$$C=2H(\alpha+\beta-k^2)\frac{(\alpha+\beta-k^2)^{5/2}}{(k^2-\beta)^2}. \quad (10)$$

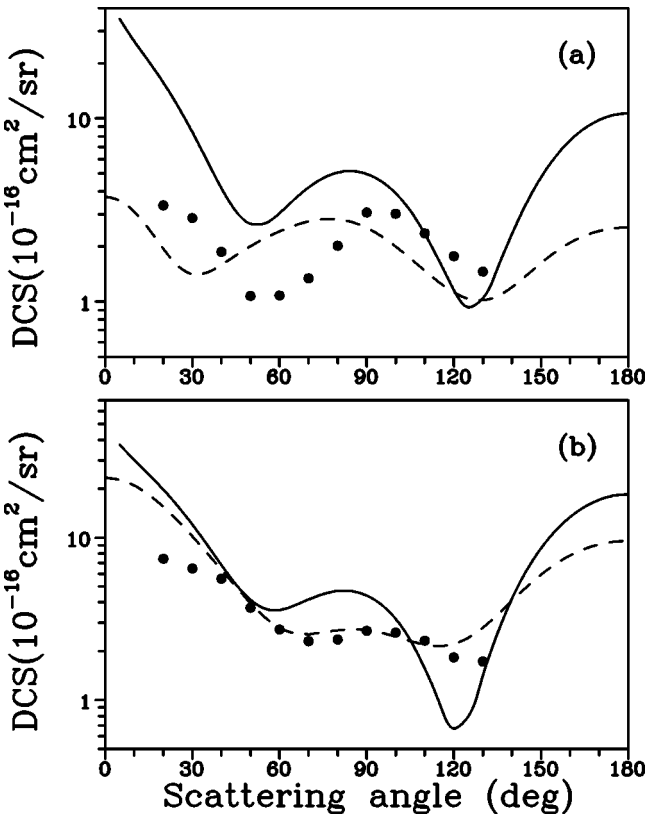

FIG. 1. DCS's for elastic e^--SiH scattering at (a) 2 eV and (b) 3 eV. Full curve: present rotationally summed results; short-dashed curve: calculated DCS's for e^--SiH_4 scattering of Lee *et al.* [31]; full circles: experimental DCS's for e^--SiH_4 scattering of Tanaka *et al.* [32].

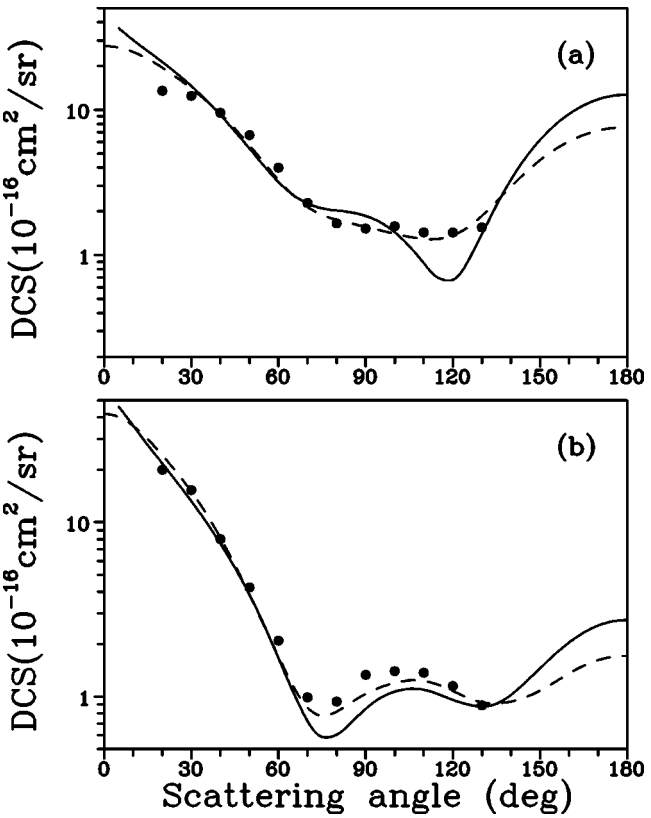

FIG. 2. Same as Fig. 1 but for (a) 5 eV and (b) 10 eV.

In Eqs. (6)–(10), k^2 is the energy (in rydbergs) of the incident electron, k_F the Fermi momentum, and $\rho(\vec{r})$ the local electronic density of the target. $H(x)$ is a Heaviside function defined by $H(x)=1$ for $x \geqslant 0$ and $H(x)=0$ for $x<0$. According to Staszewska *et al.* [28],

$$\alpha(\vec{r},E)=k_F^2+2(2\Delta-I)-V^{SEP} \tag{11}$$

and

$$\beta(\vec{r},E)=k_F^2+2(I-\Delta)-V^{SEP}, \tag{12}$$

where Δ is the average excitation energy and I is the ionization potential. As suggested by Jain and Baluja [29], the ionization potentials of SiH and SiF were used as the average excitation energy in this work.

In principle, the Lippmann-Schwinger scattering equation for elastic e^--radical scattering with the entire complex optical interaction potential can be solved using the SVIM. Nevertheless, a tremendous computational effort would be required, particularly due to the large number of coupled equations involved, which makes such calculations practically prohibitive. On the other hand, our calculation has re-

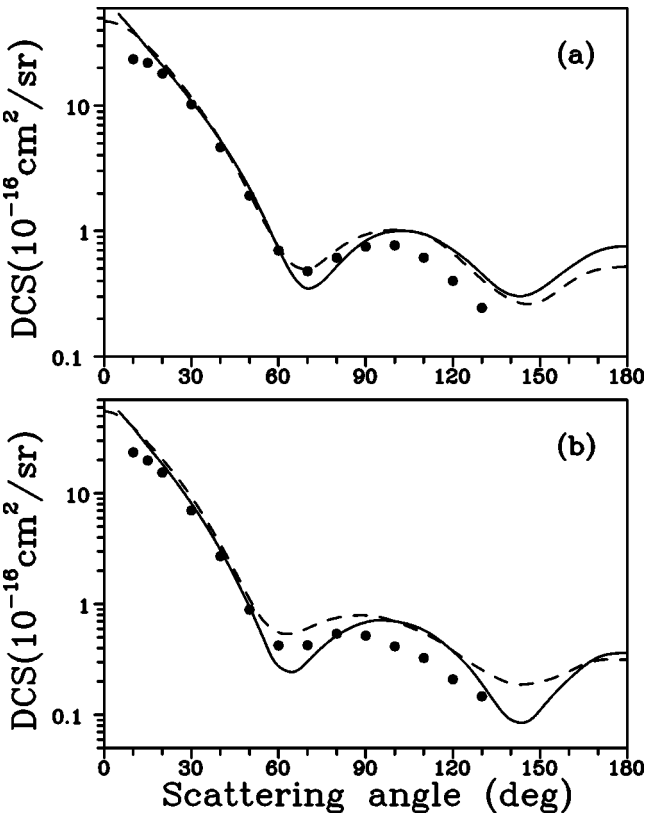

FIG. 3. Same as Fig. 1 but for (a) 15 eV and (b) 20 eV.

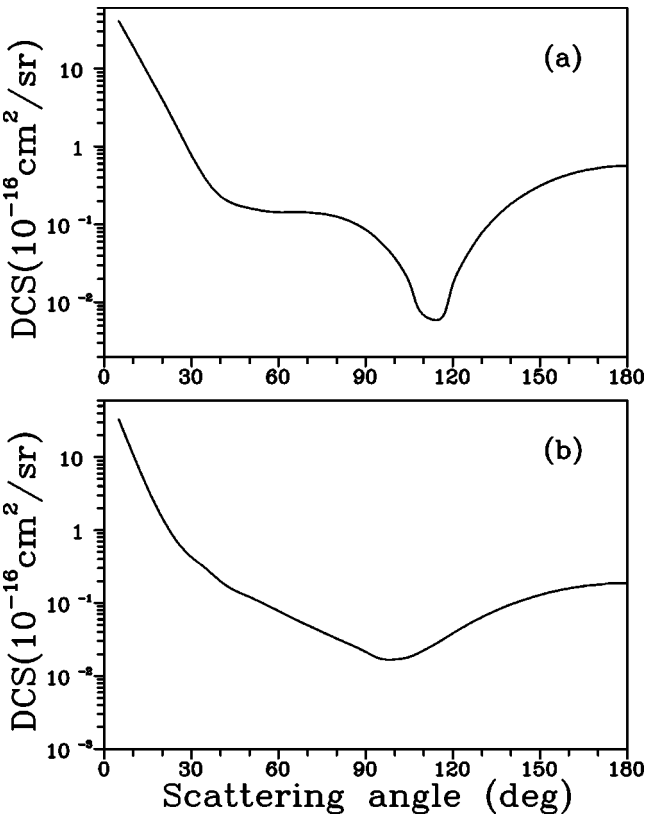

FIG. 4. Same as Fig. 1 but for (a) 80 eV and (b) 200 eV.

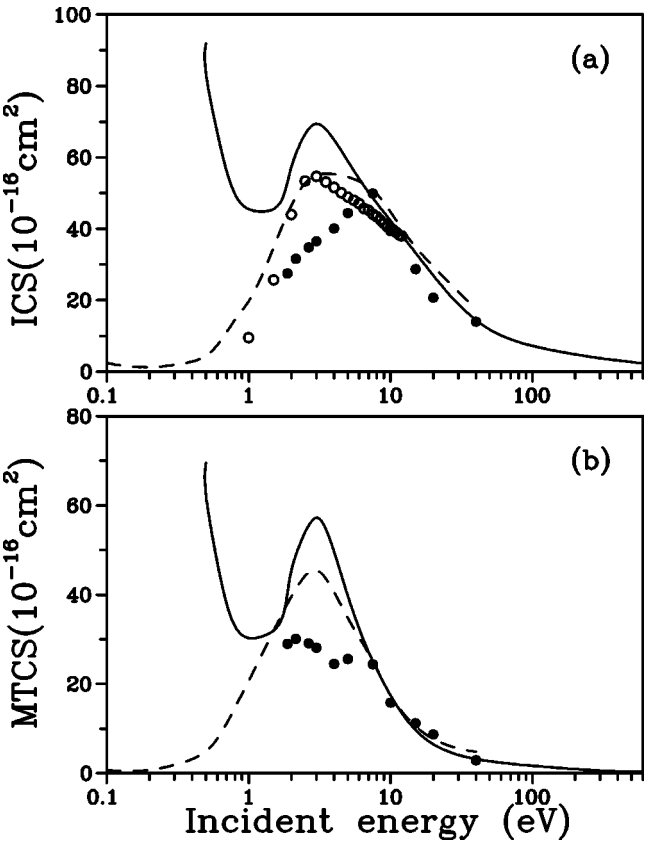

FIG. 5. (a) ICS's and (b) MTCS's for elastic electron scattering by SiH in the 1–500 eV range. Full curve: present rotationally summed results; dashed line: calculated results for e^--SiH_4 scattering of Lee *et al.* [31]; full circles: experimental results for e^--SiH_4 scattering of Tanaka *et al.* [32]; open circles: experimental results of Wan *et al.* [33].

vealed that the magnitude of the imaginary part (absorption) of the optical potential is considerably smaller than its real counterpart. Therefore, in the present study, the scattering equation for elastic e^--radical collisions is solved using the SVIM considering only the real part of the optical potential. The absorption part of the T matrix is calculated via the DWA.

In SVIM calculations, the continuum wave functions are single-center expanded as

$$\chi_{\vec{k}}^{\pm}(\vec{r})=\left[\frac{2}{\pi}\right]^{1/2}\sum_{lm}\frac{(i)^l}{k}\chi_{klm}^{\pm}(\vec{r})Y_{lm}(\hat{k}), \tag{13}$$

where the superscripts $(+)$ and $(-)$ denote the incoming-wave and outgoing-wave boundary conditions, respectively. Moreover, the absorption part of the T matrix is written as

$$T_{abs}=i\langle\chi_f^-|V_{ab}|\chi_i^+\rangle. \tag{14}$$

Since SiH and SiF are open-shell radicals with the ground-state configurations $X^2\Pi$, two spin-specific scattering schemes (the singlet and triplet couplings) between the scattering electron and the isolated 1π electron of the target are considered in the present study. Therefore the statistical average of the elastic scattering DCS's is written as

$$\frac{d\sigma}{d\Omega}=\frac{1}{4}\left[3\left(\frac{d\sigma}{d\Omega}\right)^1+\left(\frac{d\sigma}{d\Omega}\right)^0\right], \tag{15}$$

where $(d\sigma/d\Omega)^1$ and $(d\sigma/d\Omega)^0$ are the multiplet-specific DCS's for the total (e^-+target) spin $S=1$ (triplet) and $S=0$ (singlet) couplings, respectively.

In this study, the wave functions of ground-state targets are obtained using a ROHF SCF calculation. At the experimental equilibrium geometry, $R_{Si—H}=2.8726$ a.u. and $R_{Si—F}=3.0257$ a.u. [30], the calculated ROHF SCF energy and the dipole moment are $-289.356\ 93$ a.u. and 0.287 D for SiH, and -388.3223 a.u. and 0.981 D for SiF, respectively.

In the present study, we have limited the partial-wave expansion of the continuum wave functions as well as of the T-matrix elements up to $l_{max}=50$ and $m_{max}=17$. Since both radicals are polar, the partial-wave expansions converge slowly due to the long-range dipole interaction potential. Therefore, a Born-closure formula is used to account for the contribution of higher partial-wave components to the scattering amplitudes. Accordingly, Eq. (3) is rewritten as

$$\langle jm_j|f|j_0m_{j_0}\rangle = 4\pi[(2j+1)(2j_0+1)]^{1/2} i \sum_{ll'm} (-1)^{m+m_{j_0}+1} i^{l-l'} (T_{ll'm} - T^{Born}_{ll'm}) Y_{l'm_j-m_{j_0}}$$

$$\times \sum_L (2L+1)^{-1} (l0l'm_j - m_{j_0}|ll'Lm_j - m_{j_0})(l-ml'm|ll'L0)$$

$$\times (j-m_jj_0m_{j_0}|jj_0Lm_{j_0}-m_j)(j0j_00|jj_0L0) + \langle jm_j|f^{Born}|j_0m_{j_0}\rangle, \quad (16)$$

where $T^{Born}_{ll'm}$ are the partial-wave expanded T-matrix elements. They are calculated using the first Born approximation. For a rotating dipole, they are given by

$$T^{Born}_{ll'm} = -\frac{D}{L}\left[\frac{(L+m)(L-m)}{(2L+1)(2L-1)}\right]^{1/2}, \quad (17)$$

where $L=l'$ when $l'=l+1$ and $L=l$ when $l'=l-1$. In addition, for $j_0=0$, the full LF Born electron-scattering amplitude for a rotating dipole with dipole moment D is given by

$$f^{Born} = \frac{2D}{q}\left[\frac{4\pi}{3}\right]^{1/2} i \sum_m D^1_{m0}(\hat{R}) Y_{1m}(\hat{q}'), \quad (18)$$

where $\vec{q}' = \vec{k}'_0 - \vec{k}'_f$ is the momentum transferred during the collision. Further, rotationally summed cross sections are obtained by summing up the contributions of individual rotational excitation cross sections. Sufficient rotational states were included to ensure the convergence to be within 0.2%. In addition, the TCS's are calculated using the optical theorem.

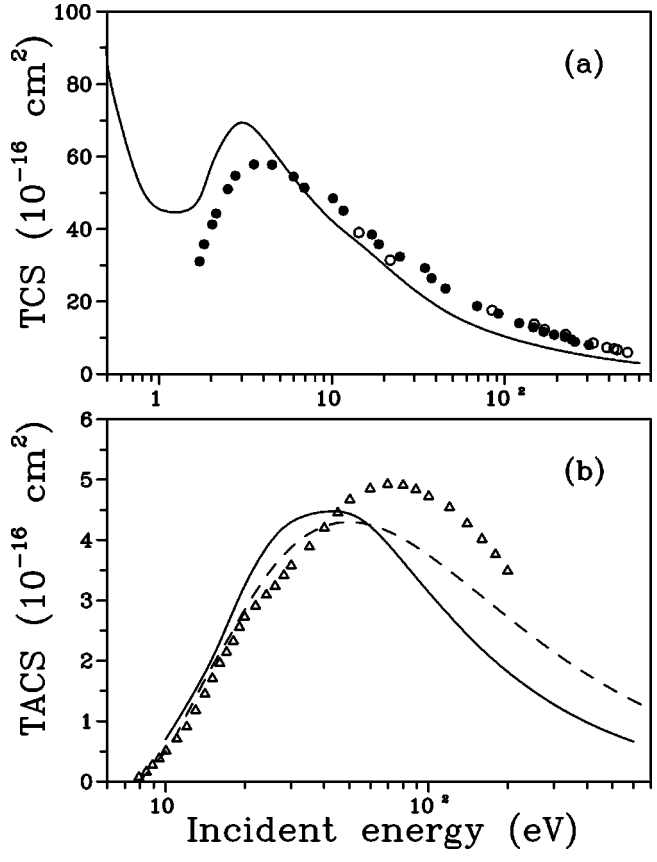

FIG. 6. (a) TCS's for electron scattering by SiH in the 1–500 eV range. Full curve, present calculated results. The experimental TCS's for e^--SiH_4 scattering are full circles: measured results of Zecca *et al.* [35]; open circles: measured results of Szmytkowski *et al.* [36]. (b) TACS's for electron scattering by SiH in the 1–500 eV range. Full curve: present calculated results, dashed line: calculated BEB TICS results of Ali *et al.* [34]; open triangles: experimental TICS's of Tarnovsky *et al.* [9].

III. RESULTS AND DISCUSSION

A. Electron scattering on SiH radical

In Figs. 1–4 we show our calculated DCS's (rotationally summed) for elastic e^--SiH scattering in the 2–200 eV en-

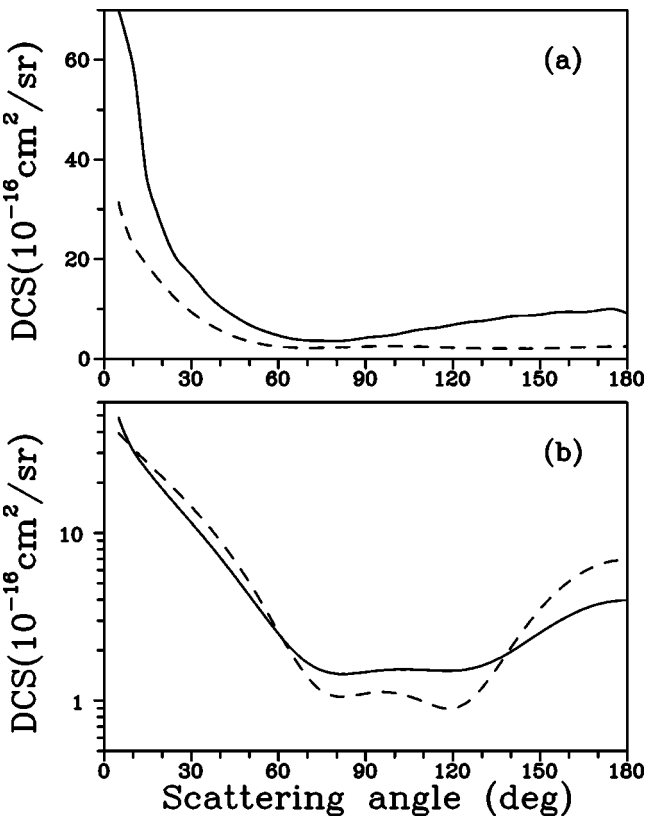

FIG. 7. DCS's for elastic e^--SiF scattering at (a) 1 eV and (b) 7 eV. Full curve: present rotationally summed results; dashed curve: corresponding calculated DCS's for e^--SiH scattering.

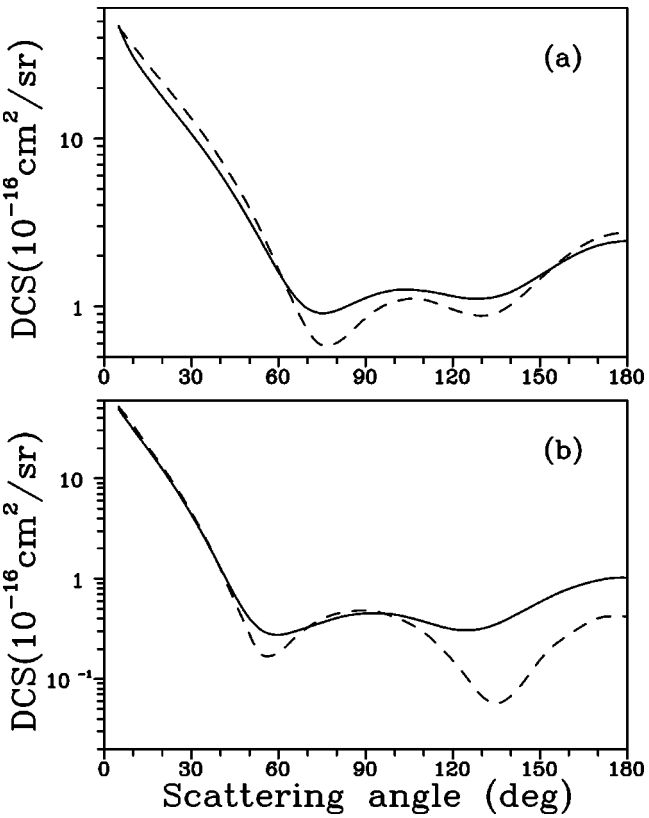

FIG. 8. Same as Fig. 7, but for (a) 10 eV and (b) 30 eV.

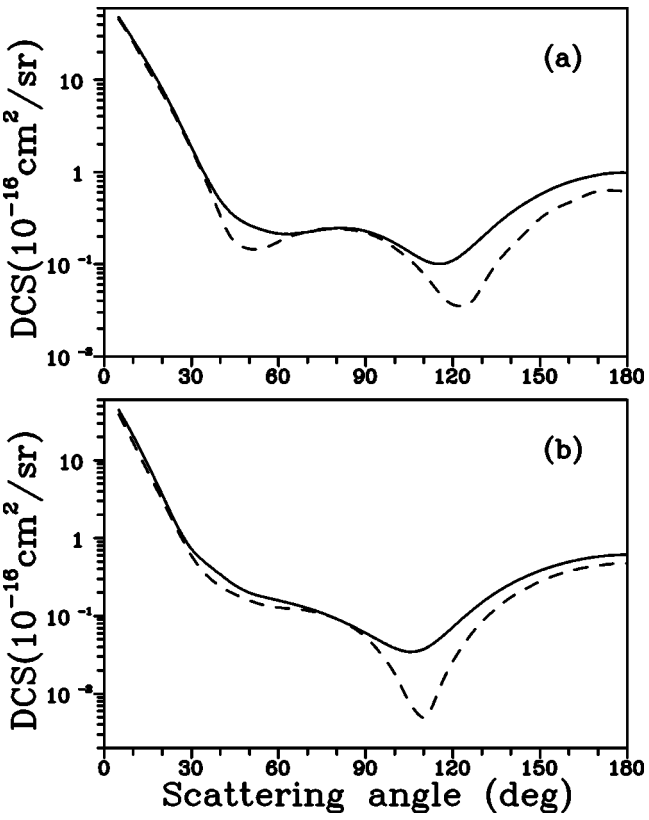

FIG. 9. Same as Fig. 7, but for (a) 50 eV and (b) 100 eV.

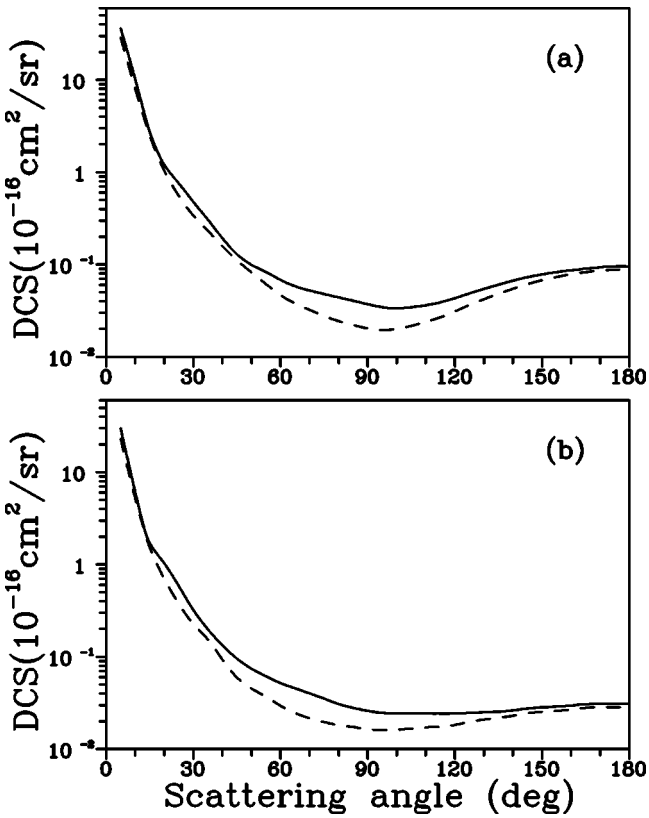

FIG. 10. Same as Fig. 7, but for (a) 300 eV and (b) 500 eV.

ergy range. Since there are no experimental or other calculated data available in the literature to be compared with our data, the calculated [31] and measured [32] results for elastic e^--SiH_4 collisions at some selected incident energies were used for comparison. This procedure has already been adopted recently by us for the e^-–CH/CH_4 collisions [15]. As in the e^-–CH/CH_4 case, we note that at 10 eV and above, the DCS's for electron scattering by SiH and SiH_4 are very similar, both qualitatively and quantitatively. Even at incident energy as low as 2 eV, there is a qualitative agreement between the DCS's for e^--SiH scattering and those of e^--SiH_4 collisions, which clearly indicates that the electron scattering by the central silicon atom dominates the interaction dynamics for these targets. The effect of the loss of hydrogen atoms is not important, since the silicon atom is much heavier. On the other hand, the dipole nature of the SiH reflects on the larger DCS's of electron scattering by this radical at the lower end of incident energies.

Figures 5(a) and 5(b) show our ICS's and MTCS's for e^- collision, respectively, calculated in the 1–500 eV range. Again, the corresponding calculated [31] and experimental data [32,33] for electron-silane collisions are shown for comparison. On qualitative aspects, a maximum centered at incident energies around 3 eV is seen in both our calculated ICS's and MTCS's for e^--SiH collision and indicates the existence of a shape resonance in this energy region. A resonancelike feature is also seen at about the same incident energies in the e^--SiH_4 scattering cross sections, which strongly suggests that the e^-–silicon atom interaction is responsible for this resonance. Also, quantitatively there is a

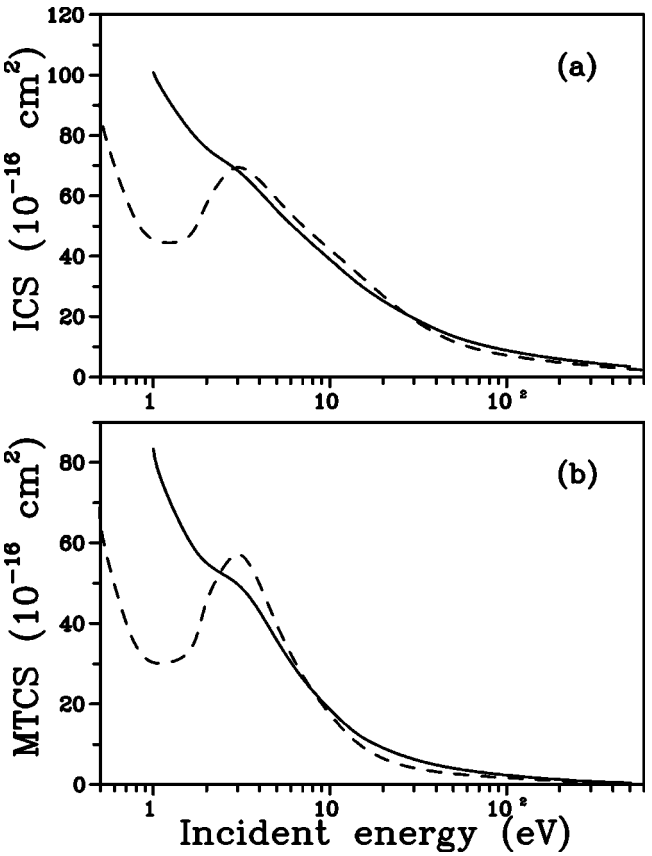

FIG. 11. (a) ICS's and (b) MTCS's for elastic electron scattering by SiF in the 1–500 eV range. Full curve: present rotationally summed results; dashed line: calculated results for e^--SiH scattering.

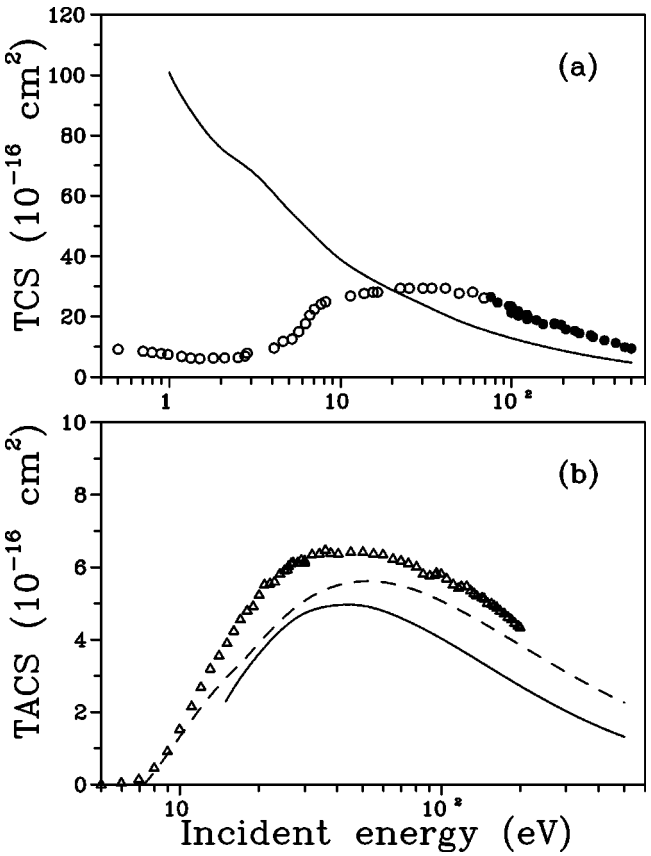

FIG. 12. (a) TCS's for electron scattering by SiF in the 1–500 eV range. Full curve: present calculated results. The experimental TCS's for e^--SiF_4 scattering are full circles: data from Trento laboratory [38]; open circles: data from Gdansk laboratory [38]. (b) TACS's for electron scattering by SiF in the 1–500 eV range. Full curve: present calculated results; dashed line: calculated BEB TICS results of Hwang *et al.* [37]; open triangles, experimental TICS's of Hayes *et al.* [10].

close similarity between the present calculated ICS's and MTCS's and those of e^--SiH_4 scattering at incident energies above 5 eV, which again indicates the dominant contribution of the electron interaction with the central silicon atom. Nevertheless, the different low-energy behavior of the cross sections for e^--SiH and e^--SiH_4 collisions, particularly for incident energies below 1 eV, reflects the dipolar nature of these targets.

Figures 6(a) and 6(b) show our TCS's and TACS's for e^--SiH collisions calculated in the 0.5–500 eV range, respectively, along with the experimental TICS's [9] and the calculated TICS's of Ali *et al.* [34] using the binary-encounter Bethe (BEB) model. Some experimental data of TCS's for e^--SiH_4 scattering [35,36] are also shown in Fig. 6(a) for comparison. In general, the qualitative similarity between the present calculated TCS's and those of the e^--SiH_4 scattering is evident. Quantitatively, our calculated SiH data also agree reasonably well with the experimental data for SiH_4 at energies above 5 eV. Again, the larger TCS's of e^--SiH scattering at lower energies is probably due to the polar nature of this radical. The comparison of our calculated TACS's and the experimental TICS's of Tarnovsky *et al.* [9] show good agreement for incident energies below 100 eV. In this energy region, good agreement is also seen between the present TACS's and the BEB TICS's of Ali *et al.* [34]. At high energies, our TACS's lie systematically below both the measured and BEB TICS's. Since the model absorption potential used in this work accounts for all inelastic open channels, including the excitation and ionization processes, our calculated TACS's should be stablished as an upper limit of the TICS's. As pointed out by Joshipura *et al.* [12], the participation of the ionization contributions to TACS's varies from 70% to 100% at incident energies around 100 eV and above. The underestimation of our results at energies above 100 eV lead us to believe that the present model absorption potential should be improved at high incident energies.

B. Electron scattering on SiF radical

In Figs. 7–10, we show our calculated DCS's (rotationally summed) for elastic e^--SiF scattering in the 1–500 eV energy range. In this case, even for elastic electron scattering on SiF_4, no measurements or calculations are available in the literature. Therefore, the calculated DCS's for e^--SiH collisions at some selected incident energies are shown to compare with the data of SiF. It is quite interesting to note that the DCS's for electron scattering by these targets show qualitative agreement even at incident energy as low as 1 eV. At 7

eV and above, quantitative agreement is also observed at small scattering angles. In general, the DCS's for e^--SiF scattering are larger, which probably reflects that fluorine atom is a better scatterer than hydrogen atom. It also reflects the larger dipole moment of SiF, particularly at low incident energies.

Figures 11(a) and 11(b) show our ICS's and MTCS's for e^--SiF collision, respectively, calculated in the 1–500 eV range along with the corresponding data for SiH. On qualitative aspects, the maximum feature seen in the ICS's and MTCS's of SiH, centered at incident energies around 3 eV, is not apparent in the ICS's of SiF. However, a shoulder at about same energies in the MTCS's of SiF indicates the existence of a shape resonance. As discussed above, we believe that this resonance is also mainly due to the electron interaction with silicon atom. It became less visible in SiF probably because of the interference of the strong dipole scattering at this low incident energies. Quantitatively, there is a close similarity between the present calculated cross sections of SiH and those of SiF at incident energies above 8 eV. On the other hand, the significantly larger ICS's and MTCS's of e^--SiF scattering below 3 eV is again due to the larger dipole moment of SiF.

Figures 12(a) and 12(b) show our TCS's and TACS's for e^--SiF collisions calculated in the 1–500 eV range, respectively, along with the experimental TICS's [10] and the calculated BEB TICS's [37]. In this case, the available experimental TCS's for e^--SiF_4 scattering [38] are also shown in Fig. 12(a) for comparison. The present calculated TCS's for e^--SiF scattering disagree even in qualitative aspects with the experimental data for e^--SiF_4 scattering. Quantitatively, at the lower end of incident energy, the TCS's for e^--SiF scattering are significantly larger, reflecting the strong dipole electron-target interaction. On the other hand, the TCS's for e^--SiF_4 scattering become larger for incident energies above 20 eV, which clearly indicates the important scatttering power of the fluorine atoms. The comparison of our calculated TACS's and the experimental TICS's of Hayes *et al.* [10] and BEB TICS's [37] show very good qualitative agreement. Quantitatively, our calculated TACS's is about 30% lower than the experimental TICS's. As discussed above, in principle our TACS's should be an upper limit of the TICS's. This underestimation clearly indicates the need of improvement of the model absorption potential.

IV. CONCLUSION

Our study on electron scattering by silicon monohydride and silicon monofluoride radicals in the low- and intermediate-energy range have revealed some interesting aspects. First, the similarity between the calculated elastic and total cross sections for e^--SiH collisions and those corresponding data for e^--SiH_4 scattering, even at incident energy as low as 2 eV, clearly shows that the electron–silicon atom interaction dominates the collisional dynamics. On the other hand, the discrepancy between our calculated TCS's for SiF target and the experimental results for SiF_4 seems to indicate the important scattering contribution of fluorine atoms. At the lower end of incident energies, the dipole interaction is dominant for both e^--SiH and e^--SiF scatterings.

The comparison of our calculated TACS's with the experimental and calculated TICS's for both targets show qualitative agreement. Nevertheless, our calculation underestimates the magnitude of cross sections up to 40%. Since the model absorption potential used in the present study accounts for all inelastic open channels including excitation and ionization processes, our TACS's should stablish as an upper limit of the TICS's. This underestimation clearly indicates the need of improvement of this model potential. Efforts in this direction is underway.

ACKNOWLEDGMENTS

This work was partially supported by the Brazilian agencies FAPESP, CNPq, and FINEP-PADCT. M.F.L. thanks FAPESP and A.M.C.S. thanks CAPES for their financial support.

[1] S. Trajmar, D. F. Register, and A. Chutjian, Phys. Rep. **97**, 219 (1983).
[2] J. Hahn and C. Junge, Z. Naturforsch. A **32A**, 190 (1977).
[3] W. Wang and N. D. Sze, Nature (London) **286**, 589 (1980).
[4] S. Ramalingam, S. Sriraman, E. S. Aydil, and D. Maroudas, Appl. Phys. Lett. **78**, 2685 (2001).
[5] S. Ramalingam, D. Maroudas, and E. S. Aydil, J. Appl. Phys. **86**, 2872 (1999).
[6] S. Sriraman, E. S. Aydil, and D. Maroudas, IEEE Trans. Plasma Sci. **30**, 112 (2002).
[7] Y. B. Dai, H. S. Shen, Z. M. Zhang, X. C. He, X. J. Hu, F. H. Sun, and H. W. Xin, Acta Phys. Sin. **50**, 244 (2001).
[8] S. T. Lee, H. Y. Pend, X. T. Zhou, N. Wang, C. S. Lee, I. Bello, and Y. Lifshitz, Science **287**, 104 (2000).
[9] V. Tarnovsky, H. Deutsch, and K. Becker, J. Chem. Phys. **105**, 6315 (1996).
[10] T. R. Hayes, R. C. Wetzel, F. A. Baiocchi, and R. S. Freund, J. Chem. Phys. **88**, 823 (1988).
[11] K. N. Joshipura and M. Vinodkumar, Phys. Lett. A **224**, 361 (1997).
[12] K. N. Joshipura, M. Vinodkumar, and P. M. Patel, J. Phys. B **34**, 509 (2000).
[13] K. L. Baluja, N. J. Mason, L. A. Morgan, and J. Tennyson, J. Phys. B **33**, L677 (2000).
[14] K. L. Baluja and A. Z. Msezane, J. Phys. B **34**, 3157 (2001).
[15] M.-T. Lee, M. F. Lima, A. M. C. Sobrinho, and I. Iga, J. Phys. B **35**, 2437 (2002).
[16] M.-T. Lee, I. Iga, L. M. Brescansin, L. E. Machado, and F. B. C. Machado, Phys. Rev. A **66**, 012720 (2002).
[17] R. R. Lucchese, G. Raseev, and V. McKoy, Phys. Rev. A **25**, 2572 (1982).
[18] L. Mu-Tao, L. M. Brescansin, M. A. P. Lima, L. E. Machado, and E. P. Leal, J. Phys. B **23**, 4331 (1990).
[19] A. W. Fliflet and V. McKoy, Phys. Rev. A **21**, 1863 (1980).
[20] M.-T. Lee and V. McKoy, Phys. Rev. A **28**, 697 (1983).

[21] M.-T. Lee, S. Michelin, L. E. Machado, and L. M. Brescansin, J. Phys. B **26**, L203 (1993).
[22] M.-T. Lee, I. Iga, L. E. Machado, and L. M. Brescansin, Phys. Rev. A **62**, 062710 (2000).
[23] M.-T. Lee and I. Iga, J. Phys. B **32**, 453 (1999).
[24] L. E. Machado, E. M. S. Ribeiro, M.-T. Lee, M. M. Fujimoto, and L. M. Brescansin, Phys. Rev. A **60**, 1199 (1999).
[25] I. Iga, M. G. P. Homem, K. T. Mazon, and M.-T. Lee, J. Phys. B **32**, 4373 (1999).
[26] S. E. Michelin, T. Kroin, I. Iga, M. G. P. Homem, and M.-T. Lee, J. Phys. B **33**, 3293 (2000).
[27] N. T. Padial and D. W. Norcross, Phys. Rev. A **29**, 1742 (1984).
[28] G. Staszewska, D. W. Schwenke, and D. G. Truhlar, Phys. Rev. A **29**, 3078 (1984).
[29] A. Jain and K. L. Baluja, Phys. Rev. A **45**, 202 (1992).
[30] *Handbook of Chemistry and Physics*, edited by D. V. Lide, 73rd ed. (CRC Press, Boca Raton, FL, 1993).
[31] M. T. Lee, L. E. Machado, and L. M. Brescansin, J. Mol. Struct.: THEOCHEM **464**, 79 (1999).
[32] H. Tanaka, L. Boesten, H. Sato, M. Kimura, M. G. Dillon, and D. Spence, J. Phys. B **23**, 577 (1990).
[33] H.-X. Wan, J. H. Moore, and J. A. Tossel, J. Chem. Phys. **91**, 7340 (1989).
[34] M. A. Ali, Y.-K. Kim, W. Hwang, N. M. Weinberger, and M. E. Rudd, J. Chem. Phys. **106**, 9602 (1997).
[35] A. Zecca, G. P. Karwasz, and R. S. Brusa, Phys. Rev. A **45**, 2777 (1992).
[36] Cz. Szmytkowski, P. Mozejko, and G. Kasperski, J. Phys. B **30**, 4363 (1997).
[37] W. Hwang, Y.-K. Kim, and M. E. Rudd, J. Chem. Phys. **104**, 2956 (1996).
[38] G. P. Karwasz, R. S. Brusa, A. Piazza, A. Zecca, P. Mozejko, G. Kasperski, and Cz. Szmytkowski, Chem. Phys. Lett. **284**, 128 (1998).